Dynamical and structural properties of undercooled Cu-Ti melts investigated by neutron and x-ray diffraction

Lucas P. Kreuzer,[1,2,*] Fan Yang,[1] Zachary Evenson,[1,2] Dirk Holland-Moritz,[1] Andrea Bernasconi,[3] Thomas C. Hansen,[4] Malte Blankenburg,[5] Andreas Meyer,[1,4] and Winfried Petry[2]

[1]*Institut für Materialphysik im Weltraum, Deutsches Zentrum für Luft- und Raumfahrt (DLR), 51170 Köln, Germany*

[2] *Heinz Maier-Leibnitz-Zentrum, Technische Universität München, Lichtenbergstraße 1, 85748 Garching, Germany*

[3]*European Synchrotron Radiation Facility (ESRF), 71 Avenue des Martyrs, 38043 Grenoble, France*

[4]*Institut Laue-Langevin (ILL), 71 Avenue des Martyrs, 38042 Grenoble, France*

[5]*Deutsches Elektronen-Synchrotron (DESY), Notkestraße 85, 22607 Hamburg, Germany*

(Received 7 February 2024; accepted 22 March 2024; published 9 May 2024)

We investigate temperature-dependent dynamical and structural properties of Cu-Ti melts within a compositional range of 24–69 at.% Ti. Accurate data of viscosity, density, and structure have been obtained by employing the electrostatic levitation technique, which enables containerlessly processing of the samples. Within the Cu-Ti system, the viscosity features a nonmonotonous trend, with the melt of the highest viscosity located at the compositions with intermediate Ti contents. This compositional trend of the liquid dynamics is not reflected in the average packing fraction derived by the macroscopic density, which is almost independent of the Ti concentration. By studying the melt structure using x-ray and neutron diffraction, particularly the direct access of the concentration-concentration structure factor S_{CC}, we show that the slowdown of the melt dynamics upon mixing is rather due to chemical effects associated with the preferred formation of Cu-Ti pairs. This leads to a contraction of the interatomic distances, whereas the almost ideal mixing behavior in the molar volume of the melt is a result of the simultaneous decrease of the average coordination number.

DOI: 10.1103/PhysRevB.109.174108

I. INTRODUCTION

Bulk metallic glasses based on Cu-Ti combine properties such as a good thermal and electric conductivity, high strength, large elastic limit, good resistance against corrosion, and biocompatibility, which can be applied in many industrial applications [1–7]. However, it was found that the glass forming ability (GFA) is very limited for Ti-rich alloy compositions [2,8]. Only alloying additional elements like Zr and Ni allows for bulk glass formation. Very recently, another class of a quasiternary systems (Ti-Zr)-(Ni-Cu)-S has been developed, where the existence of an icosahedral short-range order in the liquid state has been suggested to be responsible for an enhanced GFA [7]. Besides the structural aspect, its relationship with the dynamical properties on an atomistic scale also plays an important role for an enhanced GFA. Therefore, the relevant microscopic mechanisms responsible for such good GFAs are still to be explored [9–13].

Here we discuss the dynamical and structural properties of Cu-Ti melts. The binary Cu-Ti system serves as the basis for many excellent multicomponent glass-forming alloys, while structural properties such as the structure factor can be relatively easily obtained experimentally. Therefore, it makes a good model system. Furthermore, it features a large, undercooled liquid region, which is relevant for glass formation. It might be worth noting here that also for additive manufacturing of such alloys, a large undercooling ability is beneficial as very fine grain sizes are achieved [14]. Moreover, the binary Cu-Ti system also exhibits rather unusual thermophysical properties: the volumetric and enthalpic mixing behavior appear to show different signs, i.e., with an excess volume which is close to zero or positive, whereas the enthalpy of mixing is negative [15–17]. This is in contrast to many other binary alloys, where the excess volume and the mixing enthalpy are either both positive (e.g., Fe-Cu) or negative (e.g., Al-Cu) [18,19]. Employing molecular dynamics simulations on a Lennard-Jones system, it has been revealed that the sign of the excess volume can change depending on the magnitude of the dimensionless parameter γ in the Lennard-Jones potential (with γ the strength of the attractive term can be changed), while in the same range of gamma, there is no change in the sign of the enthalpy of mixing [15]. This hints to strong attractive interactions. Thus, we intend to investigate how the dynamical and structural properties of the melt relate to each other. Especially, the interplay between the dynamics of the system (e.g., viscosity and interdiffusion) and the structural properties (e.g., packing fraction, topological, and chemical short-range order) is of fundamental interest. Moreover, the precise knowledge of these properties in the liquid may also serve as experimental input for simulations of complex processes, such as welding, casting, surface treatment, nucleation, and crystal growth [19,20].

For many metallic glass forming alloys, a dense, efficient melt packing, i.e., a high packing fraction, is considered to be responsible for sluggish dynamics. This is regarded to favor

*lucas.kreuzer@dlr.de

glass formation, in particular, when different atomic sizes are involved [21–23]. Such correlation between dense packing and slow melt dynamics has been found to be qualitatively valid for multicomponent and even for binary (e.g., Zr-Cu and Zr-Ni) systems [20,24]. While this trend may be true within some alloy systems, it cannot be considered as a general rule, especially for transition metals. For example, the melt dynamics of $Zr_{38.2}Cu_{61.8}$ is faster than that of $Zr_{64}Ni_{36}$, despite that $Zr_{38.2}Cu_{61.8}$ exhibits a smaller molar volume [24,25]. Furthermore, it has been found that for some alloy components, especially for those containing minor additions of Al and S (e.g., Zr-(Co,Ni)-Al, Ti-Ni-S, and Ti-(Cu,Ni)-S), the above-mentioned correlation cannot be applied anymore [26,27]. Since the amount of added Al or S is small, a significant impact of these additional atoms on the packing of the melt is not expected. Rather, the results suggest that chemical interactions are crucial for the dynamics of the respective alloy systems.

In the following,we investigate thermophysical (density, viscosity) and structural properties of the binary Cu-Ti melt in the range of 24–69 at.% Ti, where a good GFA is expected. The structure of the liquid alloys was studied with a combination of x-ray and neutron diffraction, giving access to the topological and chemical short-range orders in the melt. Since Cu-Ti is highly chemically reactive (especially at higher temperatures), all samples have been containerlessly processed by using the electrostatic levitation (ESL) technique [28]. This technique also allows accessing the metastable regime of the undercooled melt, which is of special interest for the discussion of structural aspects during glass formation. Further, the absence of any container or crucible results in an excellent signal-to-noise ratio during the scattering experiments. By correlating structural information with the dynamics of the Cu-Ti melt, relationships between structure and dynamics as well as the packing fraction are discussed, which contributes to the development of a fundamental understanding of the glass formation processes on the atomic scale.

II. EXPERIMENTAL

Samples of different masses were prepared by arc melting the alloy constituents (99.999 at.% Cu and 99.99 at.% Ti) in an Ar 6N (99.9999%) atmosphere for viscosity and density ($\approx$ 50 mg), x-ray diffraction ($\approx$ 100 mg), and neutron diffraction measurements ($\approx$ 500 mg). To further purify the gas, Ar was passed through an Oxisorb cartridge, and a Ti getter was molten prior to melting of each sample to remove residual contaminants (especially oxygen) in the gas. Levitation in the ESL facility was performed under high vacuum (better than 10^{-6} mbar) conditions for both thermophysical properties and diffraction measurements [28].

A. Density and viscosity measurements

The densities of $Cu_{31}Ti_{69}$, $Cu_{50}Ti_{50}$, $Cu_{54}Ti_{46}$, and $Cu_{76}Ti_{24}$ liquid droplets have been measured by determining their respective volumes (since the sample mass is well-known). This was done by recording shadow graphs of the levitated samples as a function of temperature with a high-speed camera at a frame rate of either 1000 or 2000 fps. A detailed description of this technique can be found in Ref. [29]. The obtained images were analyzed with an edge detection algorithm, where a Legendre polynomial of the order $\leqslant 6$ was applied to describe the edge curve. The area enclosed by the edge curve was then averaged over 100 images. When assuming a rotational symmetric sample shape, the volume V can be calculated as follows:

$$V = \frac{2}{3}\pi q \int_0^{\pi} \langle R(\varphi)\rangle^3 \sin(\varphi) d\varphi, \tag{1}$$

where $\langle R(\varphi)\rangle$ is the averaged edge curve and q represents a scaling factor to convert the sample volume in the pixel units into the real sample volume, obtained by calibrating the pixel size with spheres with known diameter. The obtained density values feature an accuracy of $\Delta\rho/\rho \leqslant 0.01$. More details on the calibration and the calculations can be found in Ref. [30].

The viscosity of the Cu-Ti alloys, $Cu_{31}Ti_{69}$, $Cu_{50}Ti_{50}$, $Cu_{54}Ti_{46}$, and $Cu_{76}Ti_{24}$, has been measured by the oscillating drop technique. Using ESL, surface oscillation of the liquid sample was excited via a sinusoidal electric field (0.4−2 kV) with a frequency between 130 and 180 Hz, superimposed on the levitation voltage. After the excited dipole oscillation ($P_{2,0}$ mode) had stabilized, this additional electric field was switched off, and the decay of the oscillations was recorded with a high-speed camera analogously to the density measurements at a frame rate of 2000 fps. Thereby, the sample radius $R(t)$ as a function of time was determined. As an example, $R_z(t)$ (radius in the vertical direction) of a $Cu_{31}Ti_{69}$ sample at a temperature of 850 K is displayed in Fig. 1(a). A fast-Fourier transformation (FFT) of the oscillation spectrum yields the frequency spectrum, shown in the inset of Fig. 1(a). The isolated frequency peak around 140 Hz indicates the presence of only one single oscillation mode.

To derive the decay time, the obtained $R_z(t)$ is fitted with a damped sine function: $R_z(t) = R_0 + A\exp(-t/\tau_0)\sin(\omega t + \delta_0)$. Here, R_0 is the sample radius without oscillation, A is the amplitude of the initial excitation, τ_0 represents the decay time constant, and ω and δ_0 are the frequency and the constant phase shift, respectively. Eventually, the viscosity η was calculated by Lamb's law for the $P_{2,0}$ mode [31]:

$$\eta(T) = \left(\rho R_0^2\right)/(5\tau_0). \tag{2}$$

The derivation of the melt viscosity using such a method assumes a spherical, suspended force-free liquid droplet, in which the damping is exclusively due to internal friction under laminar flow conditions. Under laboratory conditions, these assumptions are not entirely fulfilled, e.g., due to gravitational forces, the sample is not force-free and perfectly spherical [28,29,32]. Nevertheless, it has been shown that for small sample sizes (typically sample mass below 100 mg) and in the viscosity range studied here (between 10 and a few hundred mPas), the influences of such nonideal effects are negligible. Systematic deviations can be ruled out if the obtained viscosity is independent of the sample mass [29]. This is demonstrated exemplary in Fig. 1(b) for two $Cu_{31}Ti_{69}$ samples of different mass (68 and 42 mg), where the obtained viscosity values can be described by a single temperature dependence.

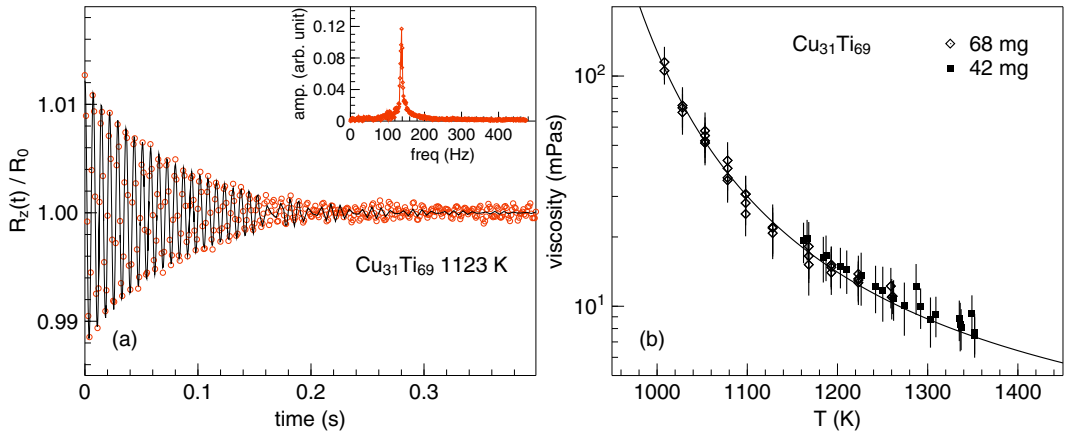

FIG. 1. (a) Normalized radius (red circles) of an undercooled liquid $Cu_{31}Ti_{69}$ sample as a function of time, depicting the decay of the oscillations measured with ESL. The black line is a fit to the data. Inset: Fast-Fourier transformation (FFT) of the decay curve. The peak indicates the excitation and eigenfrequency of the sample. (b) Viscosity η calculated via Lamb's law for samples of different masses, which can be described by a single temperature dependence.

B. X-ray diffraction

X-ray diffraction (XRD) measurements on liquid $Cu_{31}Ti_{69}$, $Cu_{33.3}Ti_{66.7}$, $Cu_{41}Ti_{59}$, $Cu_{50}Ti_{50}$, and $Cu_{54}Ti_{46}$ were performed at the ID11 beamline at the European Synchrotron Radiation Facility (ESRF) in Grenoble, France [33], and at the P21.2 beamline at the Deutsches Elektronen Synchrotron (DESY) in Hamburg, Germany, using the ESL technique. At both beamlines, the diffraction experiments were carried out in transmission geometry with approximately the same settings. A monochromatic primary x-ray beam with an energy of ∼100 keV entered the vacuum chamber of the levitator through an aluminum window of 0.5 mm thickness and ran through a Ta aperture before hitting the sample. The scattered signal passed through a second Al window (diameter of 150 mm and thickness of 5 mm) and was collected in the corner of a quadratic Frelon camera detector (ID11) or at the side of a VAREX XRD4343CT flat panel detector (P21.2), respectively. A tungsten beamstop, fixed on the inner side of the second Al window absorbed the direct beam. The detected two-dimensional diffraction images were integrated via the PYFAI software package and corrected for dark currents and detector distortions. Eventually, this yielded one-dimensional intensity $I(q)$ spectra as a function of momentum transfer q [34–36]. The total structure factor $S(q)$ was calculated from $I(q)$ after subtraction of the background of the empty levitator as well as corrections for self-absorption, multiple and Compton scattering, oblique incidence, and polarization by using the PDFGETX2 analysis software [37].

C. Neutron diffraction

Elastic neutron diffraction experiments on liquid $Cu_{31}Ti_{69}$ were performed at the high flux diffractometer D20 at the Institut Laue-Langevin (ILL) in Grenoble, France [38]. The used levitation setup is described in detail in Ref. [28]. Only for the neutron diffraction experiments, an aluminum chamber was used instead of a stainless steel chamber as in the case of synchrotron XRD experiment. The wavelength of the incoming neutrons was set to 0.94 Å. The usable angular range ($2\theta = 10-134°$) gives access to a q range from approximately 0.6 to 12 $Å^{-1}$, limited by the scattering of the primary beam (below 10°) and a positioning mirror inside the vacuum chamber (above 134°). To further reduce the background signal, an oscillating radial collimator has been used. The signal-to-background ratio is better than 10:1, achieved with the utilization of the ESL. The $Cu_{31}Ti_{69}$ alloy has an average neutron scattering length near zero [$b_{Cu} = 7.718(4)$ fm and $b_{Ti} = -3.370(13)$ fm]. According to Eq. (8), this gives the opportunity to directly obtain the partial concentration-concentration structure factor $S_{CC}(q)$ using a data treatment procedure described in detail in Ref. [39].

D. Temperature measurements

In all the levitation experiments, the temperature of the sample was measured contactless using a pyrometer operating in single color mode. To take into account the unknown (effective) emissivity, the measured pyrometer temperature T_{pyro} is corrected according to

$$1/T = 1/T_{pyro} + 1/T^{liq} - 1/T^{liq}_{pyro}, \tag{3}$$

where $1/T^{liq}$ is the liquidus temperature of the alloy and $1/T^{liq}_{pyro}$ is the liquidus temperature measured by the pyrometer [40]. For the binary Cu-Ti system, several phase diagrams are reported in the literature, summarized in Ref. [41]. Whereas on the copper-rich side the liquidus temperatures reported are mostly consistent, on the Ti-rich side partly contradicting results exist. Here we use the phase diagram of Ref. [42] where the eutectic temperature of Ti_2Cu and β-Ti phases is 1278 K and Ti_2Cu melts congruently at 1285 K. This agrees, at best, with our observations in the synchrotron XRD experiments, where we indeed observe congruent melting of Ti_2Cu, while for the composition $Ti_{69}Cu_{31}$ already β-Ti melts as the last phase. However, there are still large uncertainties and discrepancies concerning the liquidus temperature of $Ti_{69}Cu_{31}$. Thus, for the $Ti_{69}Cu_{31}$ alloy, the calibration is performed using the eutectic temperature.

III. RESULTS AND DISCUSSION

The density of four Cu-Ti compositions, $Cu_{31}Ti_{69}$, $Cu_{50}Ti_{50}$, $Cu_{54}Ti_{46}$, and $Cu_{76}Ti_{24}$, has been measured within

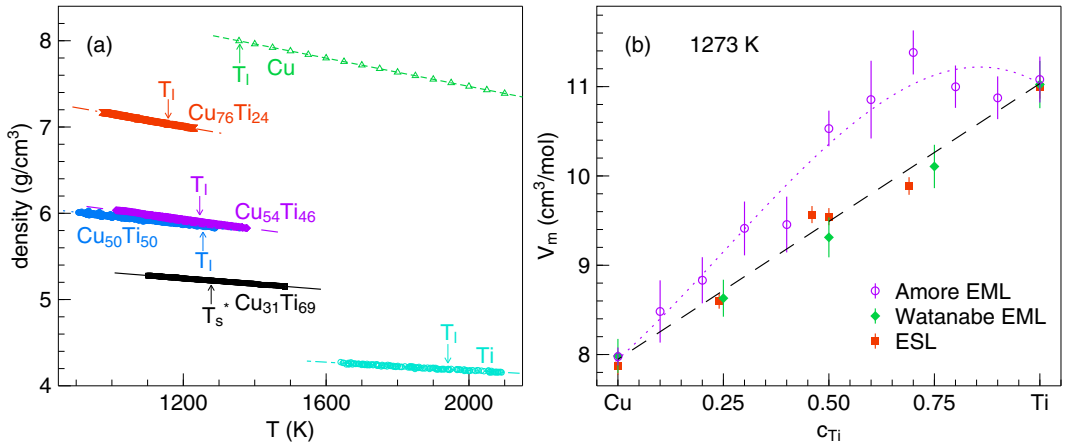

FIG. 2. (a) Temperature-dependent density of liquid Cu-Ti samples with different compositions ($Cu_{31}Ti_{69}$, $Cu_{50}Ti_{50}$, $Cu_{54}Ti_{46}$, and $Cu_{76}Ti_{24}$). The solid lines are linear fits to the data according to Eq. (4). The obtained fit parameters are listed in Table I. The values for pure Cu and Ti correspond to data reported in Refs. [43] and [44], respectively. The respective liquidus temperature of each composition (in the case of $Cu_{31}Ti_{69}$, the solidus temperature) is marked with arrows. (b) Composition dependence of the molar volume of liquid Cu-Ti samples at 1273 K obtained via ESL. In addition, the data reported in Refs. [16,17], both using EML, are shown for comparison. The dashed line represents the behavior of an ideal mixture, while the dotted line is a fit according to Eq. (5), as explained in the text [16]. The data for liquid Cu and Ti have been extrapolated.

a temperature range of 900 to 1500 K. Due to the applied ESL technique and the use of highly pure Cu and Ti during sample preparation, heterogeneous nucleation at crucible walls and within the melt, respectively, could be avoided. Thus, access to the undercooled regime with large undercooling levels of up to 300 K was possible. Figure 2(a) displays the obtained density values as a function of temperature.

The obtained density values are slightly higher than the values reported recently for the liquid Cu-Ti system by Amore *et al.* [16], which may be due to the use of electrostatic instead of electromagnetic levitation (EML). During EML, surface oscillations of the sample can be more severe and, thus, differences related to the use of the ESL and EML techniques can amount to 2−3%. They have already been observed before, e.g., for pure Ti and V [45]. Our results feature better agreement with the data reported by Watanabe *et al.* [17], who used the EML technique, however, the surface oscillation was suppressed by applying a static magnetic field. This may further confirm the origin of the observed differences. Nevertheless, both studies of Amore *et al.* and Watanabe *et al.* agree qualitatively: The density decreases upon increasing Ti content. In our paper, $Cu_{76}Ti_{24}$ features the highest density (6.8 gcm^{-3}), while $Cu_{31}Ti_{69}$ exhibits the lowest density (5.2 gcm^{-3}) at their respective liquidus or solidus temperatures (1158 K and 1278 K for $Cu_{76}Ti_{24}$ and $Cu_{31}Ti_{69}$, respectively). This seems intuitive, since Ti is a lighter element than Cu. The temperature dependence of all the obtained densities can be described by a linear fit function with a negative slope over the whole temperature range:

$$\rho(T) = \rho_L + d\rho/dT(T - T_L). \tag{4}$$

In the equation, ρ_L denotes the density at the liquidus temperature, while $d\rho/dT$ is the temperature coefficient and T_L is the liquidus temperature. The obtained values are summarized in Table I.

From the density values reported in Table I, we calculated the molar volume for each Cu-Ti composition as well as for pure Cu and Ti at 1273 K. Since this temperature is lower than the experimental temperature range for pure liquid Cu and Ti, linear extrapolation was applied to determine the molar volume. The results, displayed in Fig. 2(b), highlight an increasing molar volume upon increasing Ti content. In addition, the obtained molar volume values feature an almost ideal mixing behavior [ideal solution: dashed line in Fig. 2(b)] with small deviations for $Cu_{54}Ti_{46}$ and $Cu_{31}Ti_{69}$. The observation is in better agreement with that reported by Watanabe *et al.* [17], while Amore *et al.* found a more pronounced positive excess volume and an asymmetric behavior of the molar volume with a maximum shifted towards the titanium-rich side [16]. While typically the ESL technique provides accurate density data with very low uncertainty [46], also the agreement with the data obtained by Watanabe *et al.*, who used a static magnetic field as explained earlier, leads us to trust our data. In Fig. 2(b), the excess volume V_e as a function of the concentration of the alloy constituents and the temperature

TABLE I. Results from the fits applied to the density data shown in Fig. 2. T_{min} and T_{max} describe the temperature range, in which the density has been experimentally observed. ρ_L and $d\rho/dT$ denote the density at the measured liquidus temperature and the temperature coefficient, respectively. The data for pure Cu and Ti is taken from Refs. [43] and [44], respectively.

x_{Ti}	T_L (K)	T_{min} − T_{max} (K)	ρ_L (gcm^{-3})	$10^{-4}\, d\rho/dT$ ($gcm^{-3}K^{-1}$)
0	1358	1356−2500	8.00 ± 0.10	−8.19 ± 0.11
0.24	1158	973−1230	7.04 ± 0.07	−7.32 ± 0.08
0.46	1246	1010−1377	5.90 ± 0.06	−5.53 ± 0.06
0.50	1255	905−1289	5.85 ± 0.06	−4.71 ± 0.05
0.69	1278[a]	1100−1484	5.22 ± 0.05	−3.27 ± 0.03
1	1941	1640−2090	4.19 ± 0.06	−2.37 ± 0.30

[a]As mentioned in Sec. II, this corresponds to the eutectic temperature of the Ti_2Cu and β-Ti eutectics.

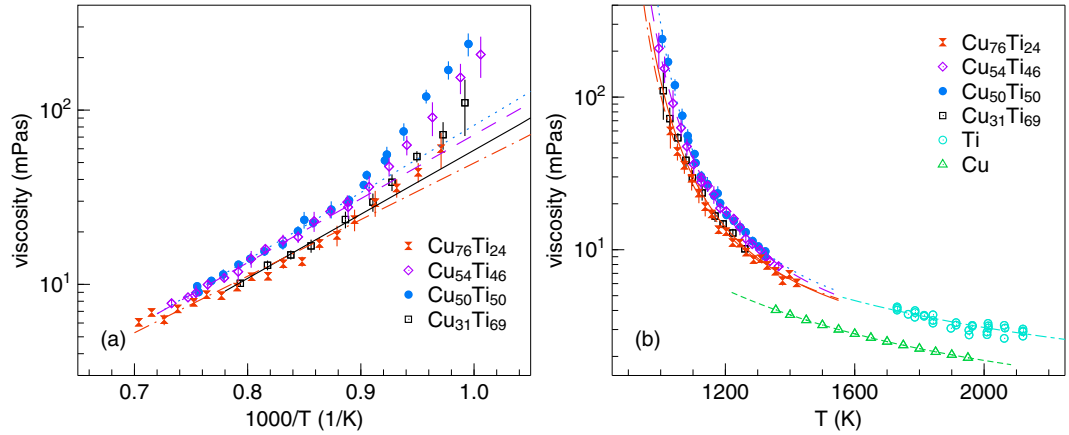

FIG. 3. (a) Arrhenius plot of the viscosity. The solid and dashed lines are Arrhenius fits and the extrapolation of the fits, respectively. (b) Viscosity as a function of temperature of liquid Cu-Ti samples with different compositions [same as in (a)]. The solid lines are Vogel-Fulcher-Tammann fits.

can be modeled according to the equation

$$V_e = x_{\mathrm{Ti}} x_{\mathrm{Cu}} (v(T) + B(x_{\mathrm{Ti}} - x_{\mathrm{Cu}})). \tag{5}$$

Here, $v(T)$ is an interaction parameter between Cu and Ti, which depends linearly on temperature as a first-order approximation [16], and B is an additional fitting parameter taking account for asymmetric concentration dependencies, e.g., mismatches in the atomic radii. For the data reported by Amore *et al.*, we obtained $v(T) = 3.2 \pm 1.3$ gcm^{-3} and $B = 2.1 \pm 3.5$ gcm^{-3} [dotted line in Fig. 2(b)]. One has to note that besides the different density values obtained by EML and ESL, the densities are compared at a lower temperature (1273 K compared to 1373 K), which eventually might result in the deviating behavior of our paper and the data reported in Ref. [16].

The melt density also serves as an input parameter for the calculation of the melt viscosity of the corresponding Cu-Ti compositions according to Eq. (2). The viscosities of the liquid Cu-Ti samples are displayed in an Arrhenius plot and in a semilogarithmic scale in Fig. 3. In the studied temperature regime, the temperature dependence of the viscosity cannot be described with a single Arrhenius fit. Extrapolating the high-temperature Arrhenius fit to lower temperatures, starting at approximately $1000/T = 0.87$ K^{-1} (1150 K), the viscosity values of all Cu-Ti compositions and the Arrhenius fit differ significantly. Instead, a Vogel-Fulcher-Tammann relationship, according to Eq. (6), describes the viscosity data well over the entire temperature range. This highlights that the temperature dependence of the viscosity is more complex than a simple process linked to a certain activation energy. Furthermore, this also underlines the importance of such measurements: While it is technically challenging to measure the viscosity over a large temperature range using ESL, the obtained results provide valuable and detailed insights into the dynamics of undercooled Cu-Ti melts:

$$\eta(T) = \eta_0 \times \exp\left(E_\eta/(k_B(T - T_0)\right). \tag{6}$$

The results of the VFT fits are listed in Table II. As expected, the viscosity increases upon cooling for all Cu-Ti compositions. At low temperatures of roughly 1000 K, the viscosity reaches values between 100 ($Cu_{31}Ti_{69}$ and $Cu_{76}Ti_{24}$) and 240 mPas ($Cu_{50}Ti_{50}$), thus indicating pronounced differences of the viscosity values for the different compositions. With increasing temperature, the viscosity values of the individual compositions approach each other. At roughly 1350 K, the values are between 8 ($Cu_{31}Ti_{69}$ and $Cu_{76}Ti_{24}$) and 10 mPas ($Cu_{50}Ti_{50}$ and $Cu_{54}Ti_{46}$). Figure 4(a) depicts the viscosity as a function of Ti content at two different temperatures (1030 and 1273 K). For comparison, the viscosities of pure Cu and pure Ti have been extrapolated to the shown temperature range using literature values (data was available in a temperature range from approximately 1360 to 1960 K [43] for pure liquid Cu and between 1730 to 2120 K for pure liquid Ti [47,48]) according to the Arrhenius temperature dependence. As discussed above, the values are likely underestimated.

It can be seen that a maximum viscosity or slowest dynamics is found for intermediate Ti contents ($Cu_{54}Ti_{46}$ and $Cu_{50}Ti_{50}$), while the samples with higher and lower Ti contents feature lower viscosities (or faster dynamics). Such behavior has been observed for many other binary systems, including those exhibiting a negative excess volume, e.g., Cu-Zr, Ni-Zr, or Ti-Ni [24,26,29]. Compared to the viscosity of the binary glass-forming system $Cu_{50}Zr_{50}$ [49], the measured viscosities of $Cu_{50}Ti_{50}$ and $Cu_{54}Ti_{46}$ are in a similar range or slightly lower for $Cu_{31}Ti_{69}$ and $Cu_{76}Ti_{24}$. When compared to $Zr_{64}Ni_{36}$, all determined values are significantly lower [50]. In comparison to the viscosity of the binary and poor glass-forming Ti-Ni system, which has been measured at higher temperatures (1300 to 1500 K), the values for all Cu-Ti compositions are roughly in the same range (at 1300 K). However, they are lower than the values of the ternary and better glass-forming Ti-Ni-S system [26]. As a result, a trend of the

TABLE II. Results from the VFT fits as shown in Fig. 3(b).

Composition	η_0 (mPas)	E_η (10^{-20} J)	T_0 (K)
$Cu_{76}Ti_{24}$	1.45 ± 0.24	1.28 ± 0.18	784 ± 26
$Cu_{54}Ti_{46}$	1.11 ± 0.16	1.63 ± 0.14	770 ± 15
$Cu_{50}Ti_{50}$	1.48 ± 0.25	1.30 ± 0.14	824 ± 15
$Cu_{31}Ti_{69}$	1.27 ± 0.29	1.41 ± 0.21	780 ± 23

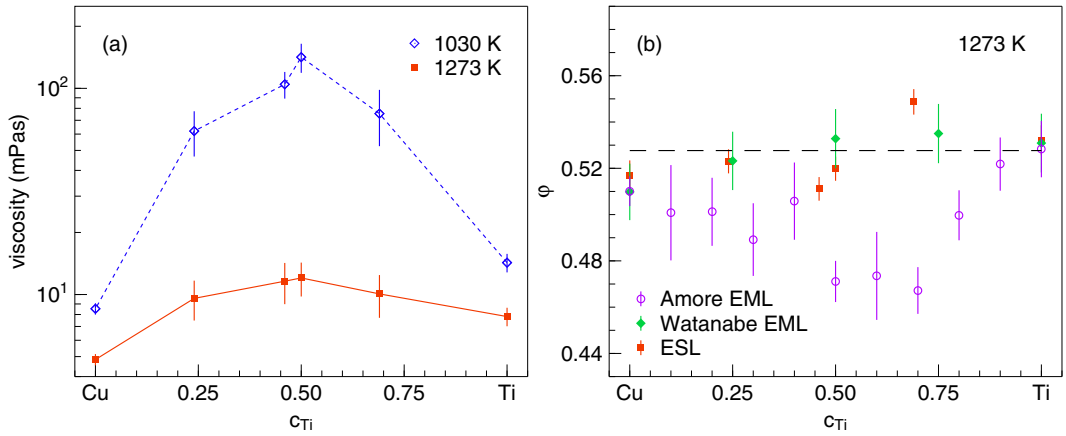

FIG. 4. (a) Isothermal values for the viscosity at 1030 and 1273 K as well as (b) packing fraction ϕ derived from different density data at 1273 K as a function of the Ti content. The black dashed line represents the here found constant packing fraction of ∼0.53, which is also in good agreement with the data reported by Watanabe *et al.* [17].

viscosity of the above-described alloy systems, regarding its impact on the GFA, cannot be extracted.

The average packing fraction can be calculated from the melt density using the covalent atomic radii of Cu and Ti ($r_{Cu} = 1.173$ Å and $r_{Ti} = 1.324$ Å, which means a radii mismatch of approximately 13%) according to Eq. (7):

$$\varphi = 4/3\pi N_{Av}\left(r_{Cu}^3 c_{Cu} + r_{Ti}^3 c_{Ti}\right)/V_M. \tag{7}$$

This has been done for different density data sets [16,17], as shown in Fig. 4(b). It should be noted that the choice of the covalent atomic radii is rather arbitrary, and there exist other definitions of atomic radii, e.g., the ionic or the Goldschmidt radius. So far, it is not clear which atomic radius best represents the size of the atoms in the metallic melts. Nevertheless, the choice of the atomic radii does not affect the compositional trend qualitatively.

For the densities obtained here by ESL and Watanabe *et al.* [17], who found a mixing behavior close to the ideal solution, the packing fraction is almost constant with an average value of ∼0.53. The average packing fraction derived from the density data reported by Amore *et al.* [16] exhibit even a minimum close to the composition $Cu_{40}Ti_{60}$. The results found in all three cases are not in line with the obtained maximum of the viscosity close to $Cu_{50}Ti_{50}$, considering the assumption that a more densely packed melt should exhibit slower liquid dynamics.

Compared to other studied binary systems, the determined values for all compositions are slightly lower than the packing fraction of Zr-Ni (e.g., $\varphi \approx 0.55$ for $Zr_{64}Ni_{36}$) [29], but similar to that of Zr-Cu (e.g., $\varphi \approx 0.53$ for $Zr_{35.5}Cu_{64.5}$) alloys [24]. However, in our case the concentration variation of the packing fraction is weak. In addition, the obtained values for all Cu-Ti compositions lie between those of the Ti-Ni and Ti-Ni-S systems. Nevertheless, given the similar atomic radii of Ni and Cu, which are neighbors in the periodic table, these differences in the liquid viscosity and average packing fraction points clearly to an impact of composition- and concentration-specific interactions between the alloy components on the atomic dynamics in these systems.

To further elaborate the relation between packing and melt dynamics, we investigated the structure of the Cu-Ti melt on a microscopic level. The total structure factors $S(q)$ of the liquid were measured with XRD experiments. The composition range from 46–69 at.% Ti has been studied, which differs slightly from the range of the density and viscosity measurements (Ti content from 24–69 at.%), with two additional alloy compositions $Cu_{41}Ti_{59}$ and $Cu_{33.3}Ti_{66.7}$. Figure 5(a) displays $S(q)$ of the investigated Cu-Ti compositions at a temperature of 1273 K, compared with the structure factor of pure Cu at 1360 K [51] and pure Ti at 1845 K [52].

The measured structure factors exhibit typical features of a disordered system with broad maxima and minima. For the alloy composition $Cu_{31}Ti_{69}$ [open squares in Fig. 5(a)], the measurement was carried out at the P21.2 beamline in a combined small- and wide-angle scattering geometry. As a consequence, the access to small q values in the wide-angle detectors was limited for $q \leqslant 2.5$ Å^{-1}. For the other alloy compositions, it can be seen that the structure factors of the Cu-Ti alloys are similar to each other, while the structure factors of Cu and Ti exhibit considerable differences in the amplitude of the first maximum, as well as the position of the second oscillation.

The x-ray scattering factors of Cu and Ti show only moderate differences (atomic numbers 29 and 22). Thus, the x-ray total structure factor is dominated by the number density structure factor S_{NN} as can be seen from Eq. (8) [54]:

$$S(q)^{BT} = \frac{\overline{b}^2}{\overline{b^2}} S_{NN} + \frac{c_A c_B (b_A - b_B)^2}{\overline{b^2}} S_{CC} + \frac{2(b_A - b_B)\overline{b}}{\overline{b^2}} S_{NC}. \tag{8}$$

Here, the concentrations of the atoms of types A and B in the melt are denoted with c_A and c_B, while b_A and b_B are the coherent scattering lengths of the atoms [in the case of XRD of the atomic scattering factors f(q)], $\overline{b} = c_A b_A + c_B b_B$ and $b^2 = c_A b_A^2 + c_B b_B^2$.

The above stated assumption is further supported by the comparatively week oscillations of the concentration-concentration partial structure factor S_{CC} determined for liquid $Cu_{31}Ti_{69}$ (see below). Hence, in this case the total x-ray structure factors allow us to derive reasonable approximations of the number-number pair correlation function g_{NN} and from this of the nearest-neighbor distances d_{NN} and the

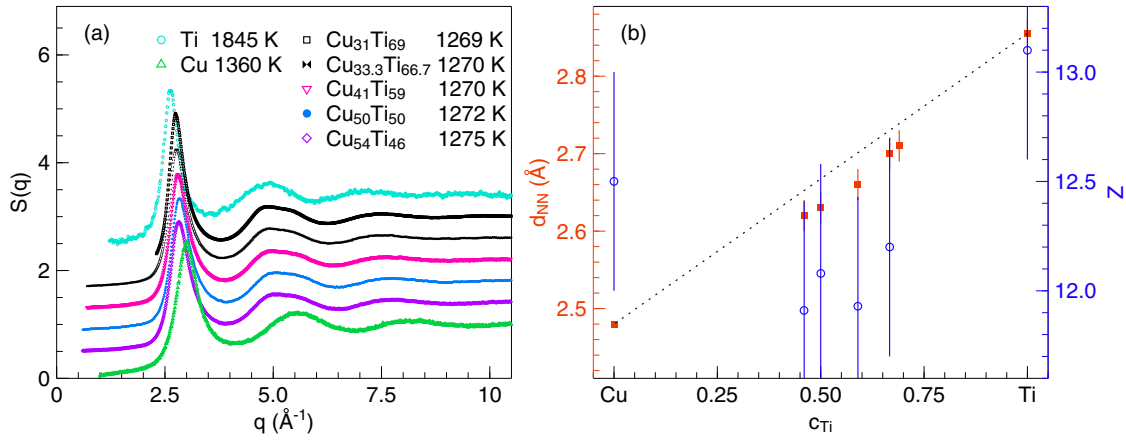

FIG. 5. (a) Total x-ray structure factor $S(q)$ of the studied Cu-Ti alloys at ∼1273 K with different compositions compared with the structure factors of pure Cu and pure Ti (Cu at approximately 1358 K [51] and Ti at 1845 K [52]). (b) Derived average interatomic distances and coordination numbers of the alloy melt at 1273 K as a function of Ti content, assuming that the total x-ray structure factors closely reassemble the number density structure factor S_{NN}.

coordination numbers Z_{NN}. The partial pair correlation functions $g_{\mathrm{NN}}(r)$ and $g_{\mathrm{CC}}(r)$ can be calculated from $S_{\mathrm{NN}}(q)$ and $S_{\mathrm{CC}}(q)$ essentially by Fourier transformation:

$$g_{AA}(r) = 1 + \frac{1}{2\pi^2 \rho_N r} \int_0^\infty q(S_{AA}(q) - 1)\sin(qr)dq, \quad (9)$$

where $\rho_N = N_A/V_m$ denotes the number density and $A = N, C$. These are shown in Fig. 7. From $g_{\mathrm{NN}}(r)$, the nearest-neighbor distances d_{NN} can be directly inferred (positions of the first maxima). The coordination numbers Z_{NN} are calculated by integrating the first peak of the radial distribution function $4\pi\rho_N r^2 g_{\mathrm{NN}}(r)$ between its first and second minimum. There exist other ways of calculating coordination numbers resulting in differing absolute values [55]. All coordination numbers discussed in this paper (including the literature values for Cu [51] and Ti [52]) are calculated in the way described above such that the data are well comparable. The main source of errors of d_{NN} and Z_{NN} are artifacts (e.g., wiggles and/or deformations of the peaks) in $g(r)$ resulting from the limited experimentally accessible q range when calculating $g(r)$ by Fourier transformation from $S(q)$. A conservative estimate of these errors gives error limits of ±0.2 Å for d_{NN} and ±0.5 for Z_{NN}

The average interatomic distance d_{NN} and coordination number Z_{NN} are shown in Fig. 5(b) as a function of Ti content at 1273 K. It can be seen that both the interatomic distance and the coordination number of Ti is higher than that of Cu. The structure factors of Ti and Cu are obtained at higher temperatures. The coordination numbers usually decrease with increasing temperature, while the temperature dependence of the interatomic distances is rather weak [52,53] and in the range of the uncertainties shown in Fig. 5(b). The average coordination numbers of the Cu-Ti alloys are lower than the coordination numbers of the pure elements. In contrast, the average interatomic distance is smaller than the ones representing an ideal mixing behavior [dotted line in Fig. 5(b)]. Therefore, it appears that on the scale of interactomic distances, local contraction upon mixing can be observed.

This behavior is more clearly visible on the difference Δd_{NN} between the derived interatomic distance of the alloys and the concentration weighted average of the pure elements,

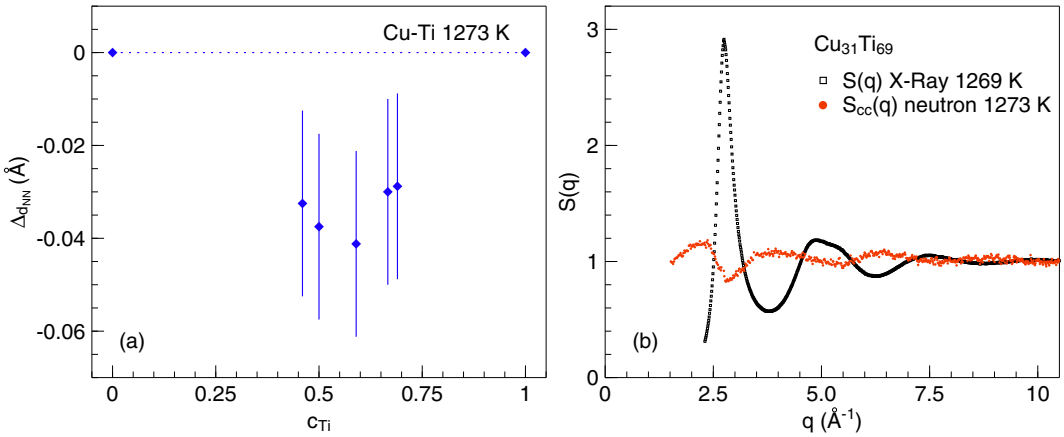

FIG. 6. (a) Differences between the derived average interatomic distances of the alloys and a weighted average of that of the pure elements. (b) Partial concentration concentration structure factor $S_{\mathrm{CC}}(q)$ measured by neutron diffraction on the zero-scattering alloy $Cu_{31}Ti_{69}$ at 1273 K compared with its x-ray total structure factor which is close to S_{NN}.

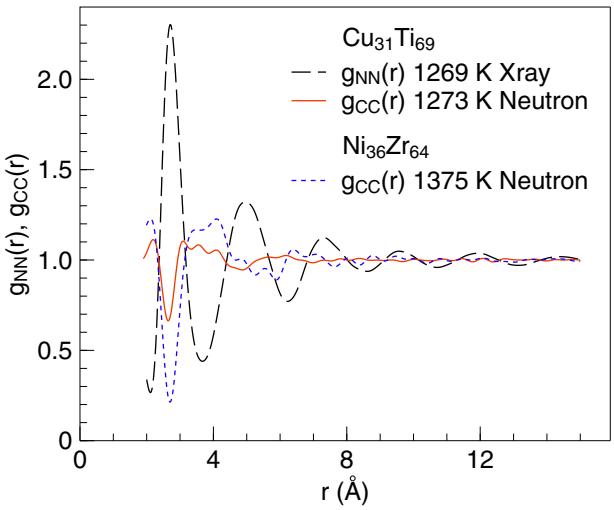

FIG. 7. Fourier transformed x-ray total structure factor of $Cu_{31}Ti_{69}$ representing in an approximation of g_{NN} and g_{CC} derived from the total and partial S and S_{CC} measured by x-ray and neutron diffraction, respectively. The g_{CC} of the $Zr_{64}Ni_{36}$ alloy melt at 1373 K is shown as a comparison.

which is smaller than zero for all the compositions studied, as shown in Fig. 6(a). On macroscopic length scales, the contraction on the interatomic distances seems to be compensated by the decrease of the average coordination number, resulting in the observed nearly ideal mixing behavior of the macroscopic density. The concentration-concentration structure factor S_{CC} according to the Bhatia-Thornton formalism measured employing neutron diffraction on the zero-scattering compositions $Cu_{31}Ti_{69}$ shows oscillations around unity indicating chemical ordering [54]. The concentration-concentration pair correlation function g_{CC} calculated by Fourier transformation from S_{CC} shows a minimum around a distance of 2.65 Å (see Fig. 7). This minimum indicates the preferred formation of heterogeneous Cu-Ti neighboring pairs. Such chemical short-range order was also observed in binary Zr-Ni and Hf-Ni alloys and is considered to induce a slowdown of the liquid dynamics [56,57]. Also, for ternary Ti-Ni-S and Zr-(Ni,Co)-Al melts [26,27], chemical interactions of the S and Al additions were suggested to result in sluggish atomic dynamics. It is, however, important to note that the maximum amplitude of the oscillations of S_{CC} seen in Fig. 6(a) is less than half of the amplitude of the oscillations found for liquid Zr-Ni or Hf-Ni [25,56,58]. Also, the minimum in g_{CC} is considerably smaller for liquid Ti-Cu than for liquid Zr-Ni or Hf-Ni. This points to a less pronounced chemical short-range order in Ti-Cu, which may provide an explanation for the faster atomic dynamics as compared with Zr-Ni or Hf-Ni melts. It may be speculated that a similar argument may also account for the faster atomic dynamics in Zr-Cu as compared with Zr-Ni. Unfortunately, here the determination of S_{CC} was not possible due to the unavailability of suitable isotopes that provide sufficient scattering contrast.

IV. CONCLUSION

In this paper, we investigate thermophysical and structural properties of the binary Cu-Ti melt in the range of 24–69 at.% Ti. Processing the samples without any crucible using ESL allows us to determine these quantities in the undercooled melt precisely. The density of the Cu-Ti system increases monotonously upon increasing the Ti content, from which an almost ideal mixing behavior of the molar volume has been identified. The melt viscosity features a nonmonotonous trend with increasing Ti content, which is largest for intermediate Ti contents close to the $Cu_{50}Ti_{50}$ composition. On the microscopic scale, local contraction of the average interatomic distance has been observed upon alloying. However, the average packing fraction derived from the macroscopic melt density remains almost constant. Therefore, the slowdown of the melt dynamics is rather due to chemical interactions between Cu and Ti, which form preferred neighboring pairs. Nevertheless, the chemical short-range order in Ti-Cu melts is less pronounced than observed for Zr-Ni or Hf-Ni melts, which may explain the faster atomic dynamics in Ti-Cu as compared with Zr-Ni and Hf-Ni.

For Cu-Ti, some structural features like the topological and chemical short-range orders can be qualitatively described by Lennard-Jones potentials [15,16]. However, the liquid dynamics depend critically on the partial liquid structure factors, and therefore on the exact shape, i.e., peak positions and oscillation amplitudes of the total structure factor. Already, small changes there lead to large changes of the liquid dynamics. Besides the relationship between the structure and dynamics in the different liquid Cu-Ti alloys provided by the present paper, the use of the ESL technique provides precise structure and dynamic data. Based on these, more realistic interatomic potentials for molecular dynamics simulation can be developed for these melts [59–61]. In combination with increasing computational power and recently developed approaches including, e.g., machine learning, this will allow future complementary studies. Thereby, remaining questions regarding the binary Cu-Ti system, e.g., the composition dependence of the diffusion coefficient, the local structure and next-neighboring atoms, and nucleation phenomena, can be answered, which eventually contribute to a deeper understanding of the relationship between structure, dynamics, and GFA. A computational study that addresses these questions is currently in progress.

ACKNOWLEDGMENTS

We thank B. Adam and L. Ruschel from Saarland University as well as D. Brüggemann, N. Grund, B. Nowak, E. Ritter, and J. Wilden from DLR for support during the beamtimes at ESRF and ILL. We also would like to thank J. Brillo for critical reading of the paper. Financial support provided by the Deutsche Forschungsgemeinschaft (DFG) via Grants No. PE580/20-4 and No. YA418/1-4 is gratefully acknowledged.

[1] F. Qin, M. Yoshimura, X. Wang, S. Zhu, A. Kawashima, K. Asami, and A. Inoue, Mater. Trans. **48**, 1855 (2007).

[2] Y.-L. Wang and J. Xu, Metall. Mater. Trans. A **39**, 2990 (2008).

[3] J. Fornell, N. Van Steenberge, A. Varea, E. Rossinyol, E. Pellicer, S. Suriñach, M. Baró, and J. Sort, J. Mech. Behavior Biomed. Mater. **4**, 1709 (2011).
[4] A. Inoue and A. Takeuchi, Acta Mater. **59**, 2243 (2011).
[5] J. Fornell, E. Pellicer, N. Van Steenberge, S. González, A. Gebert, S. Suriñach, M. Baró, and J. Sort, Mater. Sci. Eng.: A **559**, 159 (2013).
[6] T.-H. Chen and Y.-K. Hsu, Comput. Mater. Sci. **117**, 584 (2016).
[7] O. Gross, L. Ruschel, A. Kuball, B. Bochtler, B. Adam, and R. Busch, J. Phys.: Condens. Matter **32**, 264003 (2020).
[8] L. Wang, L. Ma, C. Ma, and A. Inoue, J. Alloys Compd. **361**, 234 (2003).
[9] P. Gargarella, S. Pauly, M. de Oliveira, U. Kühn, and J. Eckert, J. Alloys Compd. **618**, 413 (2015).
[10] D.-M. Lee, J.-H. Sun, S.-Y. Shin, J.-C. Bae, and C.-H. Lee, Mater. Trans. **49**, 1486 (2008).
[11] X. Wu, Z. Suo, Y. Si, L. Meng, and K. Qiu, J. Alloys Compd. **452**, 268 (2008).
[12] T. Zhang, K. Kurosaka, and A. Inoue, Mater. Trans. **42**, 2042 (2001).
[13] S. Amore, J. Brillo, I. Egry, and R. Novakovic, Appl. Surf. Sci. **257**, 7739 (2011).
[14] D. Zhang, D. Qiu, M. A. Gibson, Y. Zheng, H. L. Fraser, D. H. StJohn, and M. A. Easton, Nature (London) **576**, 91 (2019).
[15] S. Amore, J. Horbach, and I. Egry, J. Chem. Phys. **134**, 044515 (2011).
[16] S. Amore, S. Delsante, H. Kobatake, and J. Brillo, J. Chem. Phys. **139**, 064504 (2013).
[17] M. Watanabe, M. Adachi, and H. Fukuyama, J. Mater. Sci. **54**, 4306 (2019).
[18] J. Brillo and I. Egry, Jpn. J. Appl. Phys. **50**, 11RD02 (2011).
[19] I. Egry and J. Brillo, J. Chem. Eng. Data **54**, 2347 (2009).
[20] S. Stüber, D. Holland-Moritz, T. Unruh, and A. Meyer, Phys. Rev. B **81**, 024204 (2010).
[21] A. Inoue, Mater. Trans. JIM **36**, 866 (1995).
[22] A. Inoue, Acta Mater. **48**, 279 (2000).
[23] A. Inoue and A. Takeuchi, Mater. Sci. Eng.: A **375-377**, 16 (2004).
[24] F. Yang, D. Holland-Moritz, J. Gegner, P. Heintzmann, F. Kargl, C. C. Yuan, G. G. Simeoni, and A. Meyer, Europhys. Lett. **107**, 46001 (2014).
[25] D. Holland-Moritz, S. Stüber, H. Hartmann, T. Unruh, T. Hansen, and A. Meyer, Phys. Rev. B **79**, 064204 (2009).
[26] J. Wilden, F. Yang, D. Holland-Moritz, S. Szabó, W. Lohstroh, B. Bochtler, R. Busch, and A. Meyer, Appl. Phys. Lett. **117**, 013702 (2020).
[27] C. C. Yuan, F. Yang, F. Kargl, D. Holland-Moritz, G. G. Simeoni, and A. Meyer, Phys. Rev. B **91**, 214203 (2015).
[28] T. Kordel, D. Holland-Moritz, F. Yang, J. Peters, T. Unruh, T. Hansen, and A. Meyer, Phys. Rev. B **83**, 104205 (2011).
[29] P. Heintzmann, F. Yang, S. Schneider, G. Lohöfer, and A. Meyer, Appl. Phys. Lett. **108**, 241908 (2016).
[30] J. Brillo and I. Egry, Int. J. of Thermophys. **24**, 1155 (2003).
[31] H. Lamb, *Hydrodynamics* (University Press, Cambridge, 1993).
[32] W. Rhim, S. K. Chung, D. Barber, K. F. Man, G. Gutt, A. Rulison, and R. E. Spjut, Rev. Sci. Instrum. **64**, 2961 (1993).
[33] A. Bernasconi, J. Wright, and N. Harker, Powder Diffr. **30**, S2 (2015).
[34] A. P. Hammersley, J. Appl. Cryst. **49**, 646 (2016).
[35] A. P. Hammersley, S. O. Svensson, M. Hanfland, A. N. Fitch, and D. Hausermann, High Press. Res. **14**, 235 (1996).
[36] J. Kieffer, V. Valls, N. Blanc, and C. Hennig, J. Synchrotron Radiat. **27**, 558 (2020).
[37] X. Qiu, J. W. Thompson, and S. J. L. Billinge, J. Appl. Cryst. **37**, 678 (2004).
[38] T. C. Hansen, P. F. Henry, H. E. Fischer, J. Torregrossa, and P. Convert, Meas. Sci. Technol. **19**, 034001 (2008).
[39] D. Holland-Moritz, T. Schenk, P. Convert, T. Hansen, and D. M. Herlach, Meas. Sci. Technol. **16**, 372 (2005).
[40] S. Nell, F. Yang, Z. Evenson, and A. Meyer, Phys. Rev. B **103**, 064206 (2021).
[41] K. Dyal Ukabhai, U. A. Curle, N. D. E. Masia, M. Smit, I. A. Mwamba, S. Norgren, C. Öhman-Mägi, N. G. Hashe, and L. A. Cornish, J. Phase Equilib. Diffus. **43**, 332 (2022).
[42] I. Ansara, V. Ivanchenko, L. Cornish, K. Ukabhai, and K. Nape, MSI Eureka **89** (2021).
[43] M. J. Assael, A. E. Kalyva, K. D. Antoniadis, R. Michael Banish, I. Egry, J. Wu, E. Kaschnitz, and W. A. Wakeham, J. Phys. Chem. Ref. Data **39**, 033105 (2010).
[44] S. Ozawa, Y. Kudo, K. Kuribayashi, Y. Watanabe, and T. Ishikawa, Mater. Trans. **58**, 1664 (2017).
[45] B. Reiplinger and J. Brillo, J. Mater Sci. **57**, 7954 (2022).
[46] J. Brillo, F. Yang, and D. Holland-Moritz, Int. J. Thermophys **45**, 558 (2024).
[47] P.-F. Paradis, T. Ishikawa, and S. Yoda, Int. J. Thermophys. **23**, 825 (2002).
[48] T. Ishikawa, P.-F. Paradis, J. T. Okada, and Y. Watanabe, Meas. Sci. Technol. **23**, 025305 (2012).
[49] L. Chen, M. Mohr, R. Wunderlich, H.-J. Fecht, X. Wang, Q. Cao, D. Zhang, Y. Yang, and J. Jiang, J. Mol. Liq. **293**, 111544 (2019).
[50] J. Brillo, A. I. Pommrich, and A. Meyer, Phys. Rev. Lett. **107**, 165902 (2011).
[51] D. Holland-Moritz, F. Yang, T. Hansen, and F. Kargl, J. Phys.: Condens. Matter **35**, 465403 (2023).
[52] D. Holland-Moritz, O. Heinen, R. Bellissent, and T. Schenk, Mater. Sci. Eng. A **449-451**, 42 (2007).
[53] T. Schenk, D. Holland-Moritz, V. Simonet, R. Bellissent, and D. M. Herlach, Phys. Rev. Lett. **89**, 075507 (2002).
[54] A. B. Bhatia and D. E. Thornton, Phys. Rev. B **2**, 3004 (1970).
[55] P. S. Salmon, J. Phys. F: Met. Phys. **18**, 2345 (1988).
[56] B. Nowak, D. Holland-Moritz, F. Yang, T. Voigtmann, Z. Evenson, T. C. Hansen, and A. Meyer, Phys. Rev. B **96**, 054201 (2017).
[57] B. Nowak, D. Holland-Moritz, F. Yang, T. Voigtmann, T. Kordel, T. C. Hansen, and A. Meyer, Phys. Rev. Mater. **1**, 025603 (2017).
[58] B. Nowak, D. Holland-Moritz, F. Yang, Z. Evenson, and A. Meyer, Phys. Rev. B **97**, 094202 (2018).
[59] J. Horbach, R. E. Rozas, T. Unruh, and A. Meyer, Phys. Rev. B **80**, 212203 (2009).
[60] H. L. Peng, F. Yang, S. T. Liu, D. Holland-Moritz, T. Kordel, T. Hansen, and T. Voigtmann, Phys. Rev. B **100**, 104202 (2019).
[61] C. Zhang, Y. Feng, H. Liu, S. Szabó, D. Holland-Moritz, Z. Evenson, F. Yang, and H. Peng, J. Non-Cryst. Solids **613**, 122348 (2023).